Hexacoordinated Bi³⁺-Based Ellagate MOF with Acid/Base Resistance Boosting Carbon Dioxide Electroreduction to Formate

*Junjun Li,[†a] Congyong Wang,[†bd] Dingjia Wang,[†c] Chenhuai Yang,[†a] Xiaoya Cui,[e] Xuejiao J. Gao [*c] and Zhicheng Zhang [*a]*

a   Tianjin Key Laboratory of Molecular Optoelectronic Sciences, Department of Chemistry, School of Science, Tianjin University & Collaborative Innovation Center of Chemical Science and Engineering, Tianjin 300072, China.

b   Joint School of National University of Singapore and Tianjin University, International Campus of Tianjin University, Binhai New City, Fuzhou 350207, China.

c   College of Chemistry and Chemical Engineering, Jiangxi Normal University, Nanchang 330022, China.

d   Department of Chemistry, Faculty of Science, National University of Singapore, Singapore 117543, Singapore.

e   Ministry of Education Key Laboratory of Protein Sciences, Beijing Advanced Innovation Center for Structural Biology, School of Life Sciences, Tsinghua University, Beijing 100084, China. Beijing Frontier Research Center for Biological Structures, Tsinghua University, Beijing 100084, China.

*Email: zczhang19@tju.edu.cn (Zhicheng Zhang)

*Email: gaoxj@jxnu.edu.cn (Xuejiao J. Gao)

Materials and methods

Reagents and materials

Ellagic acid (96%), bismuth acetate (99%), glacial acetic acid (99.5%), potassium bicarbonate ($KHCO_3$, AR), potassium chloride (KCl, AR) anhydrous ethanol (99.5%), isopropyl alcohol (99.5%), dimethyl sulfoxide (DMSO, 99.8%), and deuterium oxide (D_2O, 99.9%) were purchased from Aladdin. 5 wt% Nafion solution and Ketjen black carbon were purchased from the Fuel Cell Store. All chemicals and materials were used without further purification.

Characterization

Powder X-ray diffraction (PXRD) patterns were analyzed with a Rigaku SmartLab 9KW with Cu Kα radiation (λ = 1.542 Å) operating at 45 kV and 200 mA. Scanning electron microscope (SEM) images were taken on a SU8010 microscope. Transmission electron microscopy (TEM), high resolution TEM (HRTEM), high angle annular dark-field scanning TEM (HAADF-STEM), and energy dispersive spectroscopy (EDS) elemental mapping were conducted on an FEI Talos F200X G2 microscope operated at 200 kV. Thermogravimetric analysis (TGA) experiments were carried out on a Mettler Toledo TGA 2 thermal analysis system. X-ray photoelectron spectroscopy (XPS) was collected on an ESCALAB-250Xi spectrometer (Thermo Fisher Scientific) using Al Kα radiation. Fourier transform infrared (FT-IR) spectra were collected on a Bruker Vertex 70 FTIR spectrometer.

Synthesis of SU-101 NRs

SU-101 NRs were prepared according to a previous report with slight modification.[1] In a typical synthesis, 0.15 g ellagic acid and 0.38 g bismuth acetate were added to a mixture of water (30 ml) and glacial acetic acid (1 ml) in common borosilicate glass beakers with PTFE stirring bars. The resulting suspension (pH ≈ 2.3) was stirred under 500 rpm at room temperature for 48 h. The resulting product was collected by centrifugation at 8000 rpm for 10 min, and washed three times with water and ethanol (v:v = 1:1).

Working electrode preparation

The dried SU-101 catalyst powder (1 mg) and Ketjen black carbon (1 mg) were dispersed into a mixture of 380 μL isopropyl alcohol and 20 μL commercial 5 wt% Nafion solution, and then sonicated for 60 min to obtain a homogeneous ink. Subsequently, the 400 μL ink was uniformly coated on a Sigracet 29 BC GDL (1 × 1 cm^2) to prepare a composite with a loading density of 1 mg cm^{-2}. The coated carbon paper was then dried overnight under ambient condition.

Electrochemical measurement

All electrochemical measurements were carried out in a three-electrode system with a sealed two-compartment H-type cell which was separated by a Nafion-117 proton exchange membrane. Each compartment was filled with 40 mL $KHCO_3$ solution (0.5 mol L^{-1}). A saturated Ag/AgCl and a platinum plate (1.5 × 1.5 cm^2) were used as the reference and counter electrodes, respectively. In this work, all the potentials were

converted to the reversible hydrogen electrode (RHE) using the formula $E_{RHE} = E_{Ag/AgCl} + E^{\theta}_{Ag/AgCl} + 0.0592 \times pH$. Electrochemical measurements were performed using a CHI760E workstation. The electrolyte was thoroughly degassed by purging with CO_2 (99.999%) for 30 min with a flow rate of 20 ml min^{-1} before the electrochemical measurements, and the pH of the resulting solution was measured to be 7.4. In order to activate the working electrode and remove adsorbed gases, cyclic voltammetry (CV) was conducted 20 times in the potential range of 0.03 to -1.57 V (vs. RHE) at a scan rate of 100 mV s^{-1}. Linear sweep voltammetry (LSV) was performed in the same potential range with CV at a scan rate of 5 mV s^{-1}. The chronoamperometry (CA) was measured at different fixed potentials to evaluate the CO_2RR performance. Gas products were analyzed using a gas chromatograph (GC7900, Tianmei) equipped with flame ionization detector and thermal conductivity detector. Liquid products were determined using a 400-MHz ^1H nuclear magnetic resonance spectrum (^1H NMR, Ascend 400) with DMSO aqueous solution as the internal standard. 0.5 mL electrolyte was mixed with 0.1 mL D_2O and 0.1 mL DMSO. The 1H spectrum was measured with water suppression. The Faradaic efficiency (FE) of products was calculated using the equation FE (%) = (mF×n)/(I×t) × 100, where m is the number of transferred electrons of CO_2RR or HER, F is the Faraday constant (96485 C mol^{-1}), n is the number of moles for a given product, and Q is the total consumed charge in electrolysis.

Calculation details

All the structural optimizations and energy calculations were performed using the Vienna Ab initio Simulation Package (VASP). Projector-augmented wave pseudopotential[2-4] with Perdew, Burke and Ernzerhof (PBE) exchange-correlation functional were used and the vdW corrections were estimated in the DFT-D3BJ form.[5-7] The energy cutoff was set to 450 eV, and the convergence thresholds for the electronic structure and forces were set to 10^{-5} eV and 0.02 eV/Å, respectively. Standard Monkhorst−Pack grid samplings were employed at $1 \times 1 \times 3$ for structural optimizations.[8]
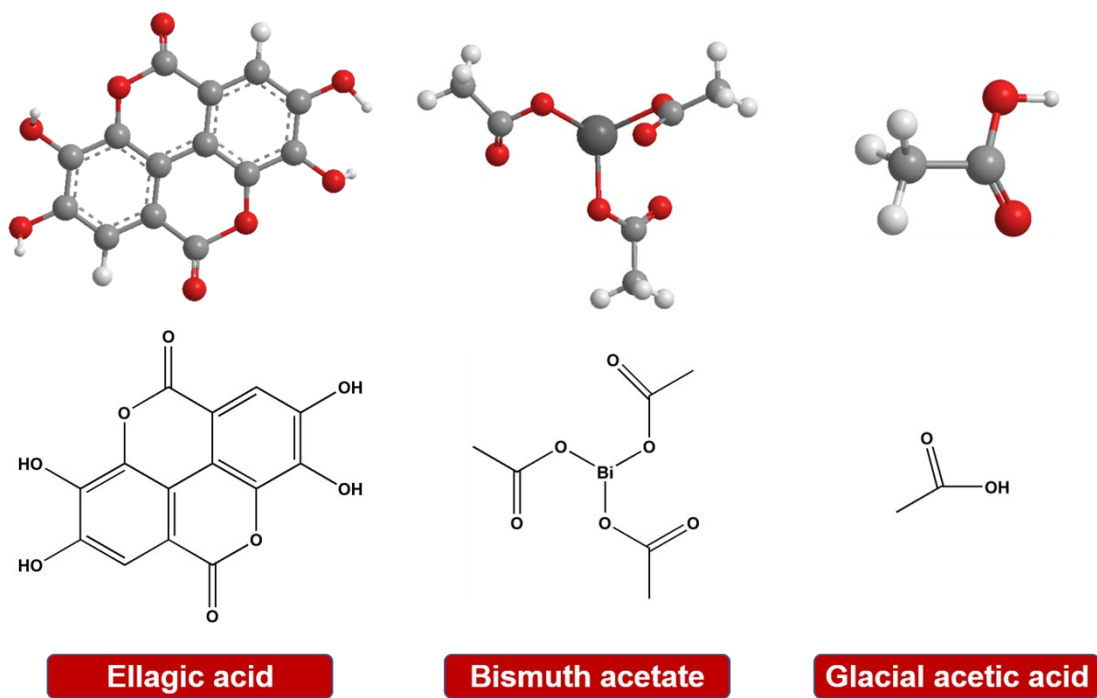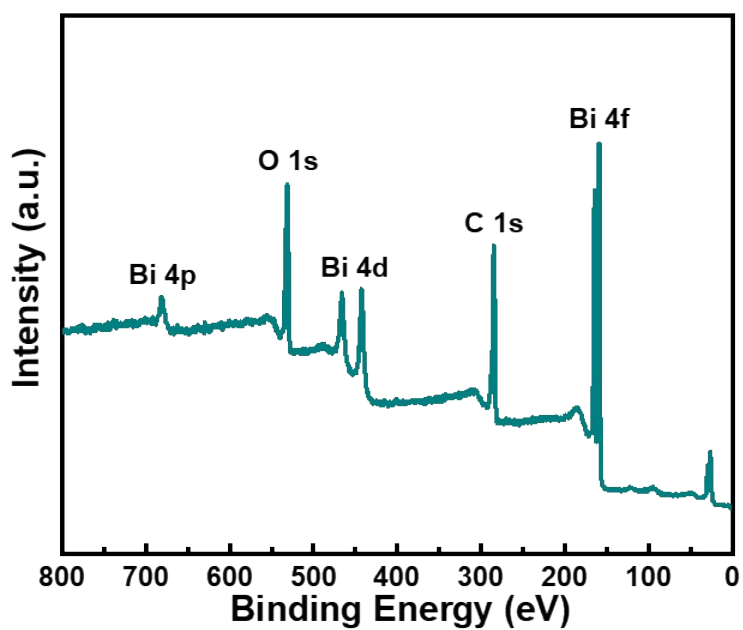
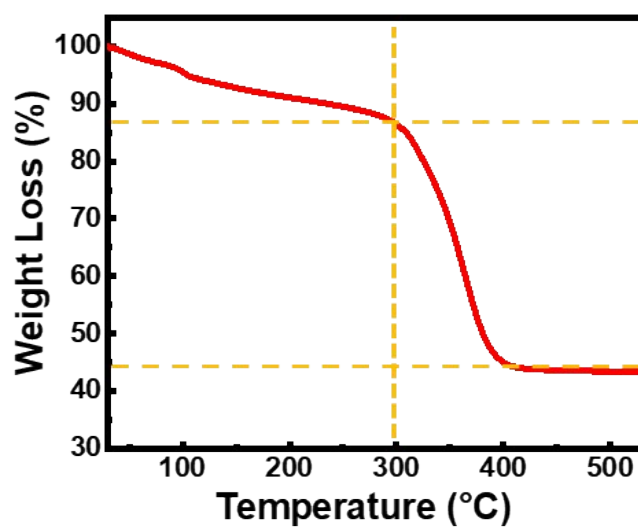**Figure S1.** The structures of ellagic acid, bismuth acetate and glacial acetic acid.
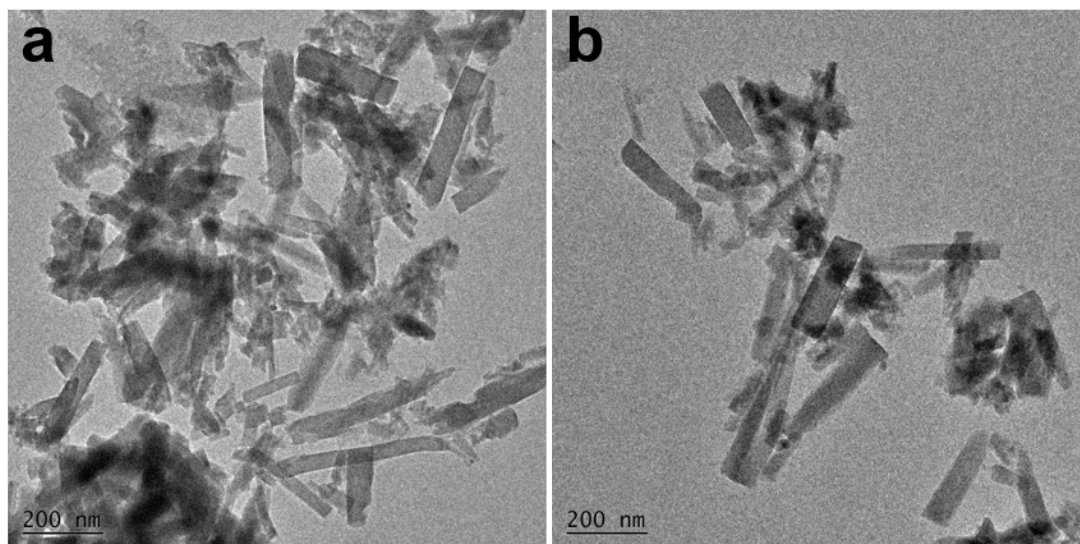
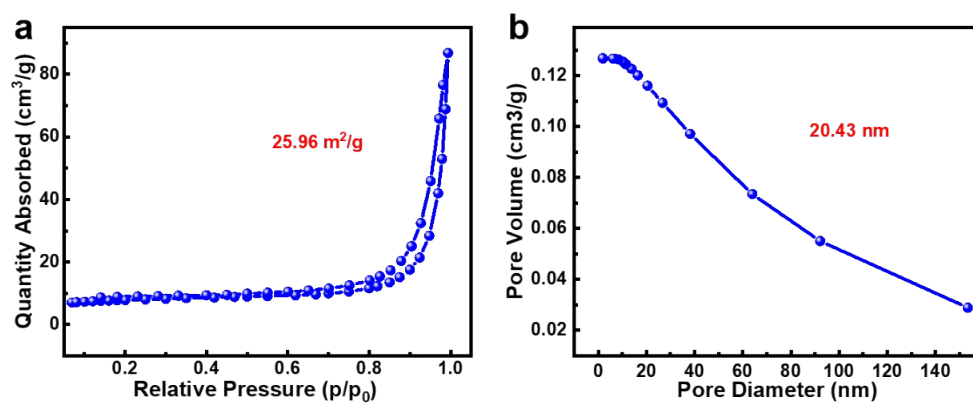**Figure S2.** TEM images of SU-101 NRs.
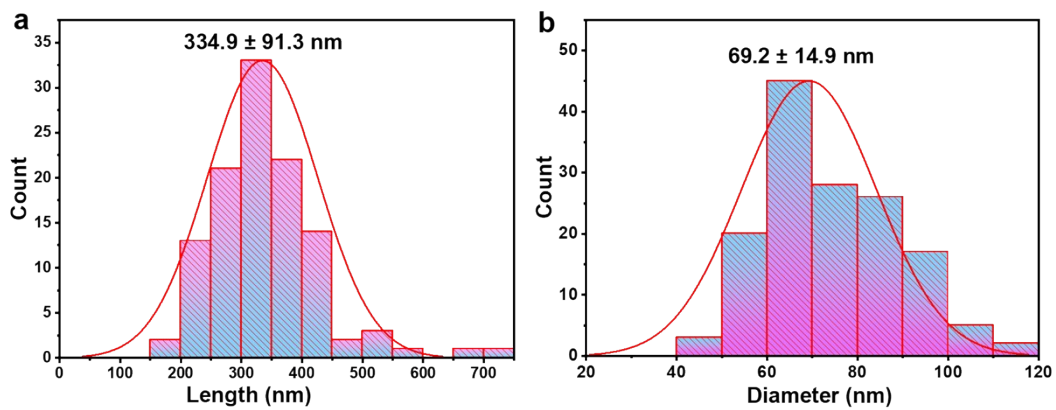
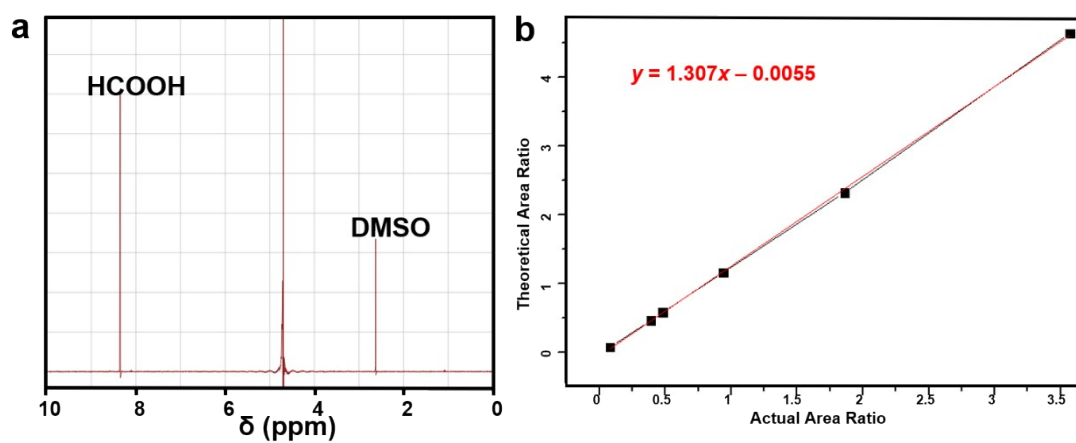**Figure S3.** The size distribution of SU-101 NRs.


Figure S4. Survey XPS spectrum of SU-101 NRs.

Figure S5. Thermogravimetric analysis profile of SU-101 NRs in air. The sample was put into a platinum crucible and heated in air from 28 °C to 600 °C with a heating rate of 10 °C min^{-1}.
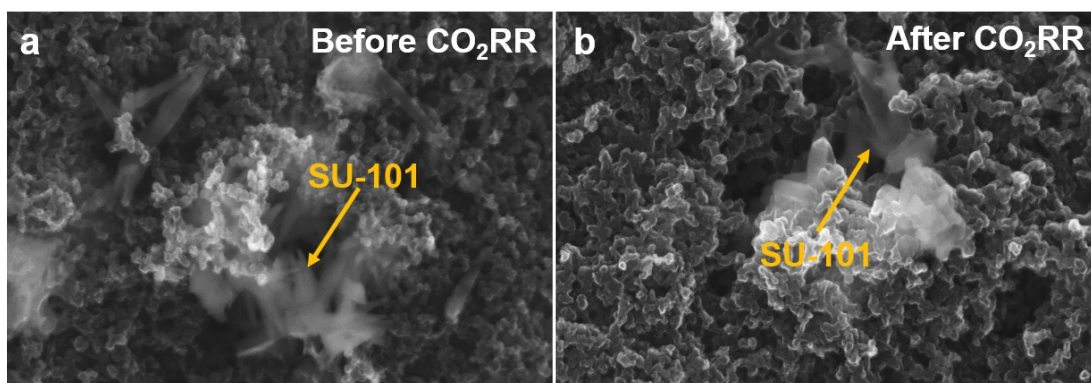

Figure S6. (a) the N_2 adsorption-desorption isotherm and (b) pore size distribution of SU-101 NRs.
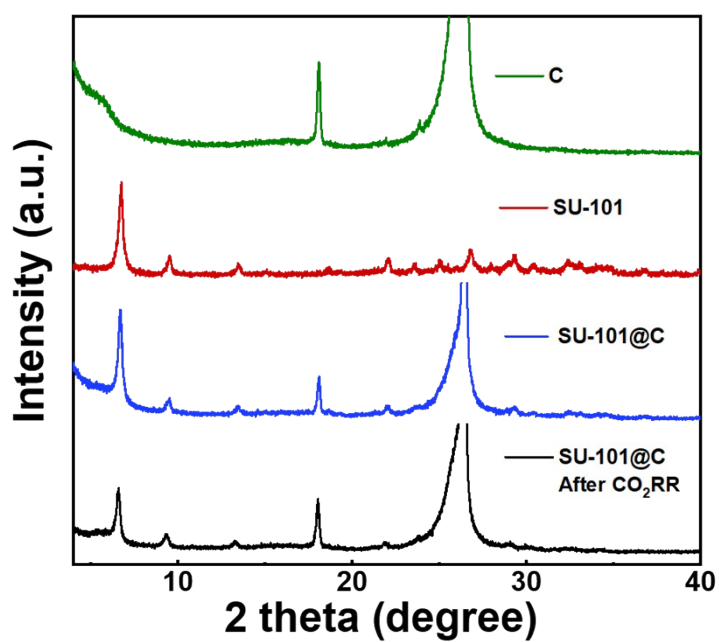
Figure S7. (a) NMR spectrum of the electrolyte after electrolysis for 1 h. (b) The linear relationship between theoretical area ration and actual area ratio.
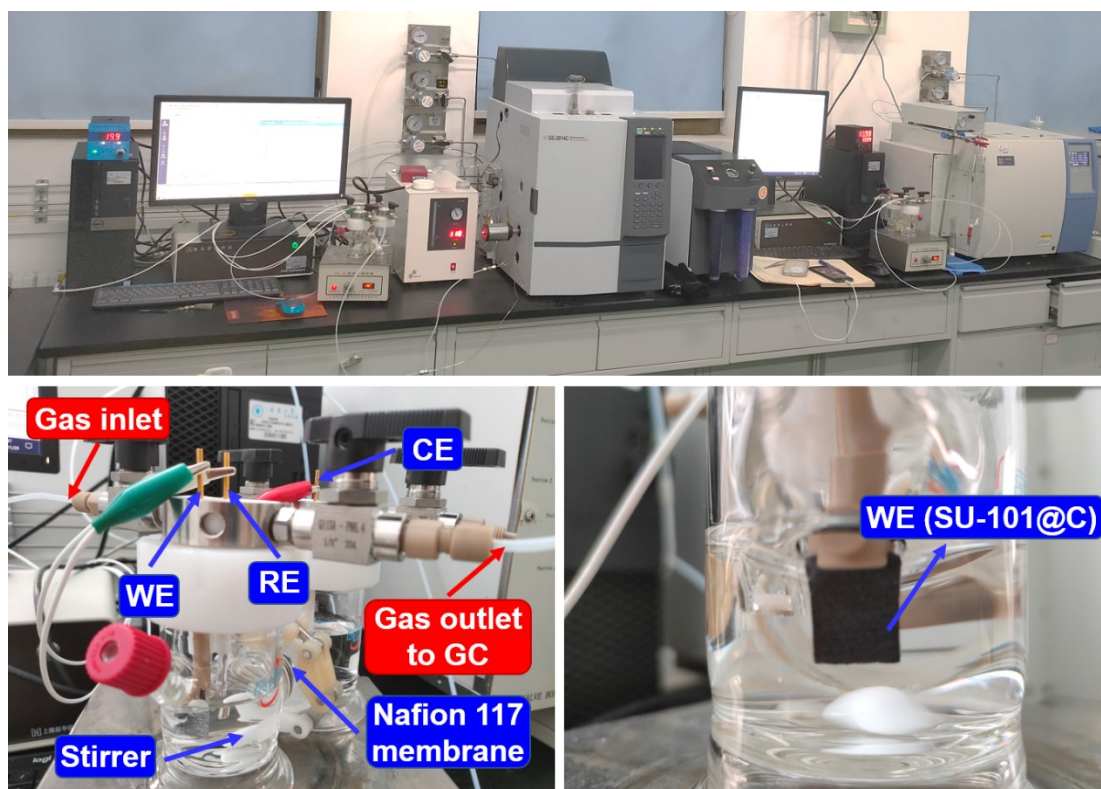
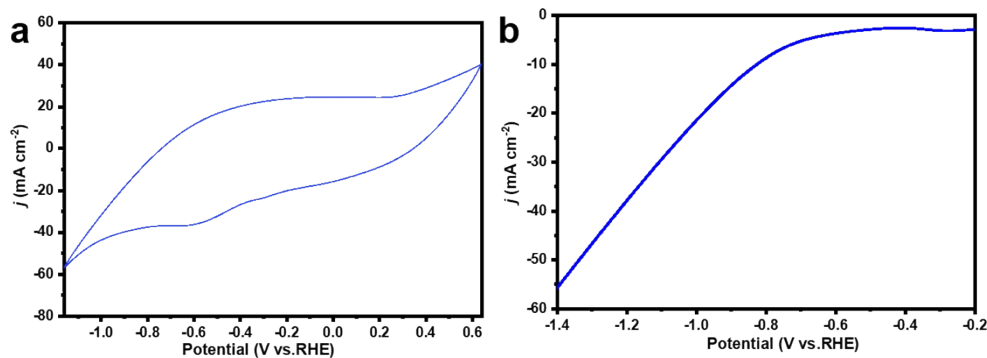**Figure S8.** Photograph of the system for electrocatalytic CO_2RR.

Figure S9. SEM images of SU-101@C catalyst (a) before and (b) after CO$_2$RR test.
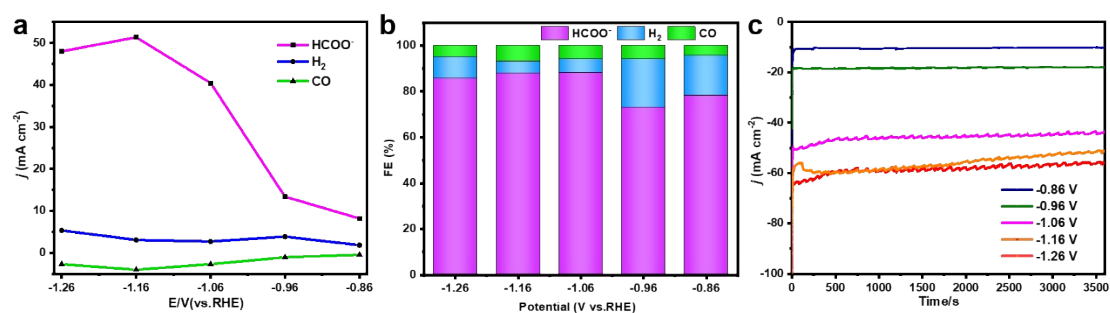

Figure S10. XRD patterns of carbon paper (C), SU-101, SU-101@C and SU-101@C (after CO$_2$RR test) catalysts.

Figure S11. (a) CV and (b) LSV curves in 1 M KOH aqueous solution at a scan rate of 5 mV s^{-1} over SU-101 catalyst for CO_2RR test in flow cell.

Figure S12. (a) Partial current densities of H_2, CO and HCOO$^-$. (b) FEs of H_2, CO and HCOO$^-$ at different applied potentials. (c) The CO_2RR test at different potentials in flow cell.
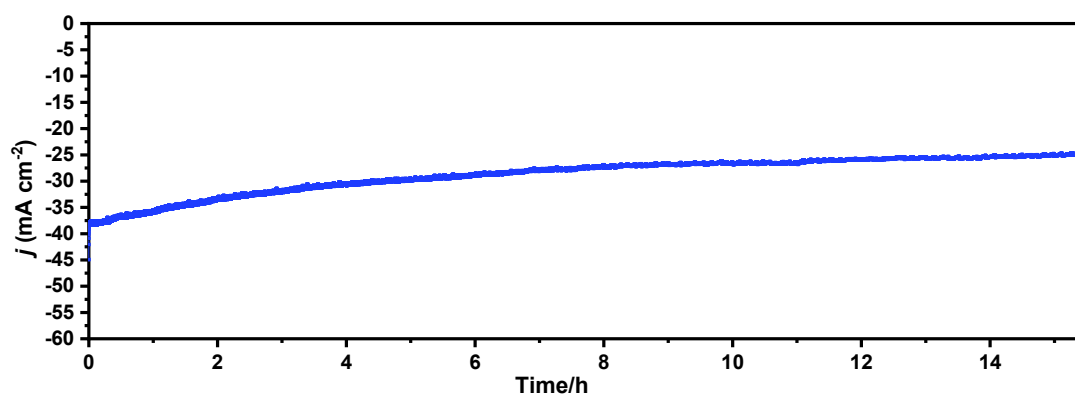
Figure S13. Total current density at -1.06 V vs. RHE over SU-101 catalyst for CO_2RR test in flow cell.
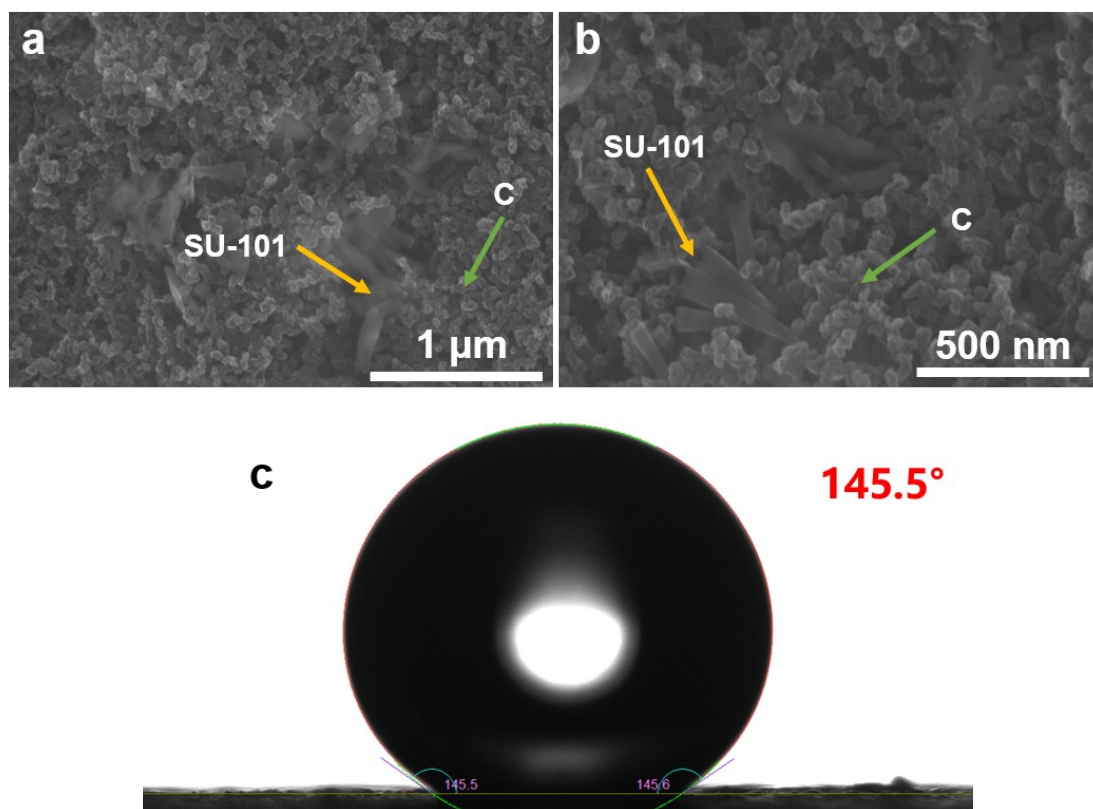
Figure S14. (a,b) SEM images of SU-101@C and (c) the contact angle between SU-101 catalyst working electrode and electrolyte.

The contact angle is 145.5°, which indicates that the electrode surface is hydrophobic and is not conducive to competing HER.

Table S1. CO$_2$RR performance of noble-metal-free catalysts for the conversion of CO$_2$ to HCOOH.

Catalyst	Electrolyte	Cell type	FE (%)	Current density (HCOOH) (mA cm^2)	Potential (V *vs.* RHE)	Reference
SU-101@C	0.5 M KHCO$_3$	H-cell	93.66	8.98 14.57	-1.06 -1.26	This work
Bi-Sn aerogel	0.1 M KHCO$_3$	H-cell	93.9	9.3	-1.0	*Angew. Chem. Int. Ed.*, 2021, **60**, 12554-12559.
Cu@SnO$_2$	0.1 M KHCO$_3$	H-cell	70.0	/	-1.45	*Adv. Mater.*, 2022, doi: 10.1002/adma.2022011 14.
Bi Nanosheet	0.05 M H$_2$SO$_4$ + 3 M KCl	Flow cell	92.2	−237.1	-1.23	*ACS Catal.*, 2022, **12**, 2357-2364.
Bi$_2$O$_3$NSs@MC CM	0.1 M KHCO$_3$	H-cell	93.8	~15	-1.256	*Angew. Chem. Int. Ed.*, 2019, **58**, 13828-13833.
Bi$_2$O$_3$@C-800	0.5 M KHCO$_3$	H-cell	93	7.5	-0.9	*Angew. Chem. Int. Ed.*, 2020, **59**, 10807-10813.
SnO$_2$	0.1 M NaHCO$_3$	H-cell	93.6	9.55	-1.07	*J. Am. Chem. Soc.*, 2014, **136**, 1734-1737.
Bi(btb)	0.5 M KHCO$_3$	H-cell	95	/	-0.97	*Adv. Funct. Mater.*, 2020, **30**, 1910408.
Bi$_2$O$_3$	0.5 M KHCO$_3$	H-cell	91	8	-0.9	*ACS Catal.*, 2019, **10**, 743-750.

Bi-Sn/CF	0.5 M KHCO$_3$	H-cell	96	/	-1.14	*Adv. Energy. Mater.*, 2018, **8**, 1802427.
Bi-SnO$_x$	0.5 M KHCO$_3$	H-cell	95.8	20.9	-0.88	*Adv. Mater.*, 2020, **32**, 2002822.
Bi NS	0.1 M KHCO$_3$	H-cell	92	/	-1.1	*Angew. Chem. Int. Ed.*, 2021, **60**, 18178-18184.
Bi-nanosheet	0.1 M KHCO$_3$	H-cell	97	8.77	-0.8	*Appl. Catal. B: Environ.*, 2020, **266**, 118625.
BiO$_x$/C	0.5 M NaHCO$_3$	H-cell	93.4	16.1	-0.92	*ACS Catal.*, 2018, **8**, 931-937.
Bi$_2$O$_3$-NGQDs	0.5 M KHCO$_3$	H-cell	98.1	18.1	-0.7	*Angew. Chem. Int. Ed.*, 2018, **57**, 12790-12794.
Bi-MOF	0.1 M KHCO$_3$	H-cell	92.2	~12.5	-0.65	*Appl. Catal. B: Environ.*, 2020, **277**, 119241.
Sn/SnO/SnO$_2$	0.5 M KHCO$_3$	H-cell	89.6	17.1	-0.9	*Nano. Res.*, 2021, **14**, 1053-1060.
Bi NSs	1 M KHCO$_3$	H-cell	95.5	/	-0.98	*Adv. Energy. Mater.*, 2020, **10**, 2001709.
Bi NTs	0.5 M KHCO$_3$	H-cell	93	36.6	-1.1	*ACS. Catal.*, 2019, **10**, 358-364.
BiNS	0.5 M NaHCO$_3$	H-cell	95	14.1	-0.67	*Nat. Commun.*, 2018, **9**, 1320.

References

1 E. S. Grape, J. G. Flores, T. Hidalgo, E. Martinez-Ahumada, A. Gutierrez-Alejandre, A. Hautier, D. R. Williams, M. O'Keeffe, L. Ohrstrom, T. Willhammar, P. Horcajada, I. A. Ibarra and A. K. Inge, *J. Am. Chem. Soc.*, 2020, **142**, 16795-16804.

2 G. Kresse and J. Furthmüller, *Comp. Mater. Sci.*, 1996, **6**, 15-50.

3 G. Kresse and D. Joubert, *Phys. Rev. B*, 1999, **59**, 1758.

4 P. E. Blöchl, *Phys. Rev. B*, 1994, **50**, 17953.

5 S. Grimme, S. Ehrlich and L. Goerigk, *J. Comp. Chem.*, 2011, **32**, 1456-1465.

6 S. Grimme, J. Antony, S. Ehrlich and H. Krieg, *J. Chem. Phys.*, 2010, **132**, 154104.

7 J. P. Perdew, K. Burke and M. Ernzerhof, *Phys. Rev. Lett.*, 1996, **77**, 3865.

8 H. J. Monkhorst and J. D. Pack, Special points for brillouin-zone integrations. *Phys. Rev. B*, 1976, **13**, 5188.